

# Ultrasonic Imaging of Textured Alumina

David B. Stang  
*Sverdrup Technology, Inc.*  
*NASA Lewis Research Center Group*  
*Cleveland, Ohio*

and

Jonathan A. Salem and Edward R. Generazio  
*National Aeronautics and Space Administration*  
*Lewis Research Center*  
*Cleveland, Ohio*

May 1989



(NASA-TM-101478) ULTRASONIC IMAGING OF  
TEXTURED ALUMINA (NASA. Lewis Research  
Center) 11 p CSCL 14D

N89-28853

Unclass  
0231758

G3/38

# ULTRASONIC IMAGING OF TEXTURED ALUMINA

David B. Stang  
Sverdrup Technology, Inc.  
NASA Lewis Research Center Group  
Cleveland, Ohio 44135

and

Jonathan A. Salem and Edward R. Generazio  
National Aeronautics and Space Administration  
Lewis Research Center  
Cleveland, Ohio 44135

## Summary

Ultrasonic images representing the bulk attenuation and velocity of a set of alumina samples were obtained by a pulse-echo contact scanning technique. The samples were taken from larger bodies that were chemically similar but were processed by extrusion or isostatic processing. The crack growth resistance and fracture toughness of the larger bodies were found to vary with processing method and test orientation. The results presented here demonstrate that differences in texture that contribute to variations in structural performance can be revealed by analytic ultrasonic techniques.

## Introduction

There is much interest in ceramics in the materials and structures research community. Researchers anticipate that many heat engine components will be manufactured from ceramics in the near future. One complication which is currently being addressed is variation in mechanical properties. Component or specimen properties can vary because of anomalies in the material such as voids, inclusions, and large grains (refs. 1, 2, and 3). Nondestructive evaluation is an important research tool for studying these anomalies since it contributes to processing optimization and to the understanding of mechanical properties (refs. 4 and 5).

Alumina is often used to study the effect of microstructure on mechanical properties since its various microstructural characteristics can be controlled in specimen fabrication. One characteristic that can be controlled is texture. Texture occurs in extrinsic and intrinsic forms. Intrinsic texture refers to a

directionality in crystallographic and grain arrangement. Extrinsic texture refers to macroscopic features: that is, the distribution and shape of anisotropic pores and impurities. Sample preparation through isostatic processing generally results in little intrinsic or extrinsic texture. However, textures will result from extrusion processing. Salem et al. (ref. 1) reported the measured effects of texture on the fracture toughness of alumina. They found that crack growth resistance was influenced by the orientation of the test sample with respect to the principal direction of the extrusion texture.

This report presents a relationship between specimen textures and ultrasonic measurements. Ultrasonic scans have been used for many years in a multitude of nondestructive testing applications. The measurements involved here, however, are more precise than those used for routine flaw detection purposes. Ultrasonic waves interact with voids, pores, inclusions, and grain boundaries of materials. The variations in fracture characteristics are governed by these factors and by texture differences that are more subtle (ref. 6). This report describes precision ultrasonic velocity and attenuation scans that reveal these subtle microstructural differences.

## Specimens

### Material Processing and Characteristics

The specimens used in this study were made from 96 percent alumina powder. Two sets of specimens were produced. One set was isostatically pressed, and the other was extruded (ref. 1). Both were then fired at 1630 °C. The effects of extrusion can be seen in the tabulation of grain and pore dimensions

(table I). For both materials, the pores and grains were similar in size, but there was a slight orientation parallel to the extrusion axis in the extruded material. This orientation can be seen in the photomicrographs (fig. 1). The long axes of the pores and grains tended to be parallel to the axis of extrusion. This slight elongation and alignment is evidence of the texture of the material.

### Toughness and Crack Growth Characteristics

The alumina fracture specimens were cut and chevron-notched for toughness and crack growth tests. The geometry and orientation of the specimens are illustrated in figure 2. The longitudinal *L* axis, the long axis of the specimen blanks, was the axis of extrusion. The isopressed as well as the extruded specimens were made such that notches were of three different orientations.

Fracture testing was performed by loading the specimens at a stroke rate of 0.05 mm/min (Bubsey, R.T.; Pierce, W.S.; and Shannon, J.L.: Generalized Wide Range Expressions for the Short Bar and Short Rod Chevron-Notched Fracture Toughness Specimens. NASA TM-83796, 1989, to be published and ref. 7). The fracture toughness  $K_{IC}$  was calculated with the equation

$$K_{IC} = \frac{P_{max} Y_{min}^*}{S(W^{1/2})}$$

where  $P_{max}$  is the maximum test load,  $S$  and  $W$  are specimen thickness and width (fig. 2(b)), and  $Y_{min}^*$  is the stress intensity coefficient, which is found from the experimental compliance relations of Bubsey et al. (NASA TM-83796).

Crack growth resistance tests were performed by gradually loading the specimen until a small increment of stable crack extension occurred. Then the specimen was unloaded. This was repeated until a crack extension of 10 mm occurred, which was the instability point. Crack growth resistance,  $K_{IR}$  was found by using the maximum load sustained and the stress intensity coefficient (Bubsey et al. NASA TM-83796).

Both fracture toughness and crack growth resistance of the extruded samples were found to vary with test orientation (table II). The toughest samples (greatest  $K_{IC}$ ) were the *RC* samples—those oriented such that the extrusion direction was perpendicular to the direction of crack growth. The sample designation refers to its orientation with respect to the longitudinal *L*, circumferential *C*, and radial *R* dimensions of the original body (fig. 2). The toughness of the *RC* extruded samples was roughly 40-percent greater than that for the isopressed material. The crack growth resistance  $K_{IR}$  was also

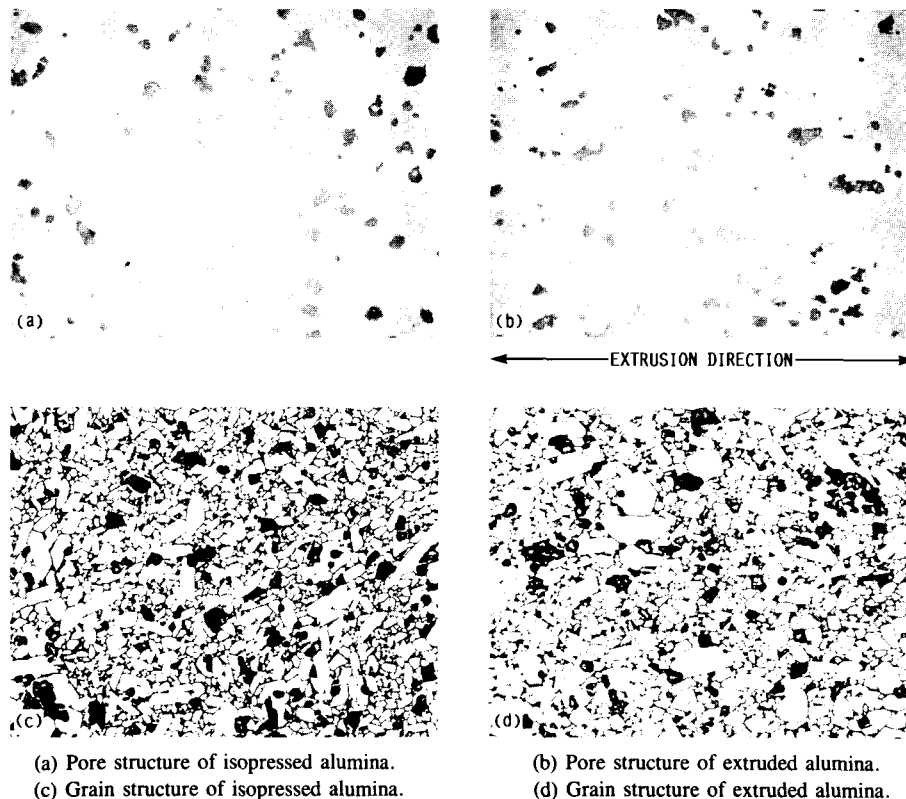
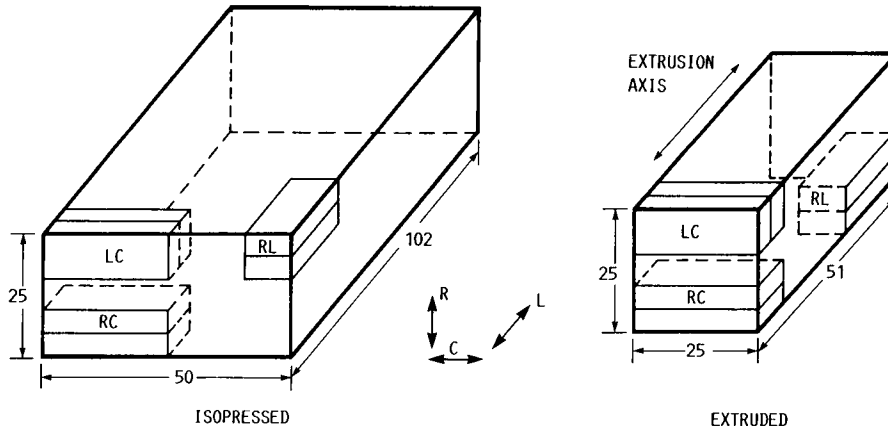
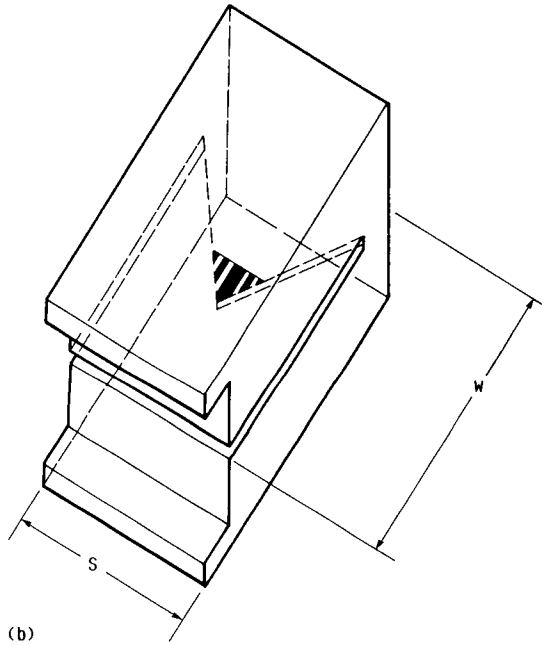


Figure 1.—Microstructure for radial-circumferential *RC* test orientations.



(a)



(b)

(a) Removal patterns for isopressed and extruded alumina specimens. All dimensions are given in millimeters.  
 (b) Geometry of alumina specimens.

Figure 2.—Geometry and orientation of alumina fracture specimens.

found to be greatest in the *RC* samples. The greater toughness resulted from interaction between the crack front and the aligned pores and grains. The crack front deviated because of the alignment, resulting in energy absorption.

Photographs of fracture surfaces clearly illustrate the texture of the extruded material (fig. 3). Ridges and valleys parallel to the extrusion direction occur across the surfaces. The surfaces of the isopressed material have no outstanding features, implying similar fracture behavior for all three orientations. The samples that were fractured such that the extrusion axis was perpendicular to the direction of crack propagation (*RC*) were tougher than those fractured in other directions.

## Ultrasonic Technique

### Velocity and Attenuation

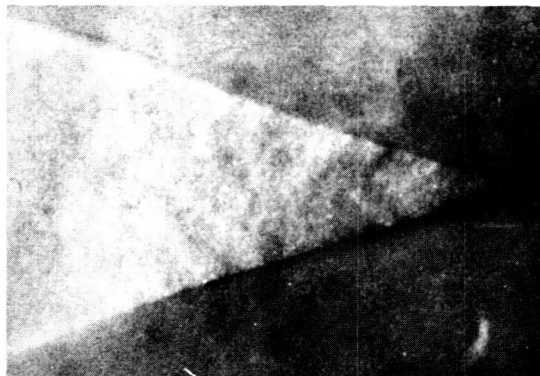
Ultrasonic pulse-echo procedures are well known (refs. 4, 5, 8, 9, and 10). The microstructure of a material influences the characteristics of a pulse as it travels through it. Pores and

grain boundaries act as scattering sites, removing energy from the pulse. Porosity also influences the speed at which the pulse travels (refs. 5 and 10). A schematic of the procedure is shown in figure 4. A broadband pulse is sent by a transducer through its buffer rod. Reflections of the pulse return from the front surface (echo  $FS_1$ ), the back surface (echo  $B_1$ ), and the back surface again (echo  $B_2$ ) after a reflection off the front surface. The Fourier transform of each waveform represents the amplitude and phase as a function of frequency. The attenuation as a function of frequency is given by

$$\alpha(f) = \frac{1}{2X} \ln \left[ \frac{|B_1(f)| |R(f)|}{|B_2(f)|} \right]$$

where

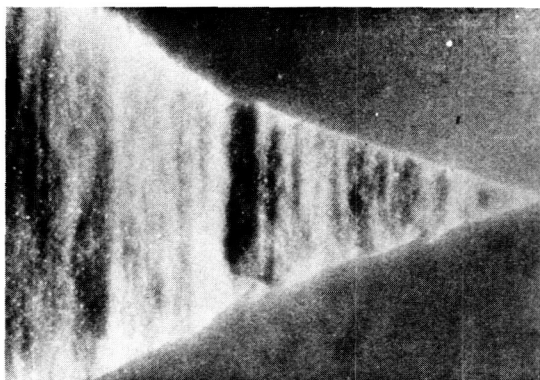
$$R(f) = \frac{|FS_2(f)|}{|FS_1(f)|}$$



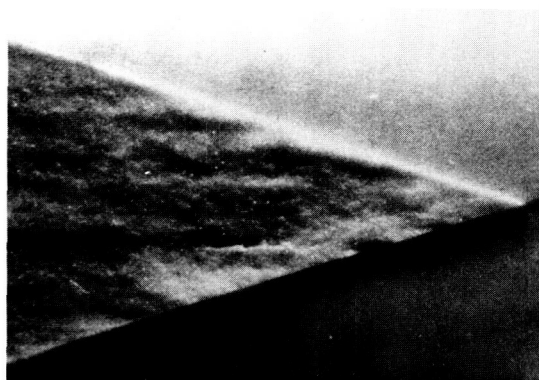
(a)



(b)



(c)



(d)

(a) Isopressed specimen.

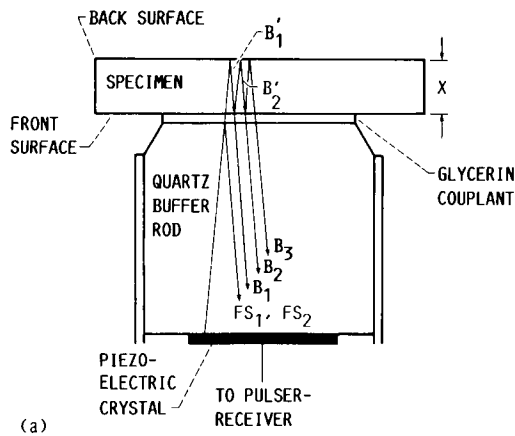
(c) Radial-circumferential *RC* orientation.

(b) Longitudinal-circumferential *LC* orientation.

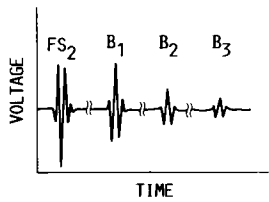
Extrusion axis perpendicular to surface.

(d) Radial-longitudinal *RL* orientation.

Figure 3.—Typical fracture topography. Arrows indicate extrusion axis.



(a)



(b)

(a) Schematic of contact pulse-echo system.

(b) Pulse echoes shown as voltage as function of time.

Figure 4.—Pulse-echo system. Echoes from front surface,  $FS_1$ ,  $FS_2$ ; echoes from back surface,  $B_1$ ,  $B_2$ ,  $B_3$ .

and

$X$  sample thickness

$FS_1$  buffer rod echo without sample in contact

$FS_2$  buffer rod echo with sample in contact

The velocity of the pulse can be found through the time interval between echoes  $B_1$  and  $B_2$ . The cross correlation velocity (refs. 9 and 11) is given by

$$\frac{2X}{\tau_0}$$

where  $\tau_0$  is the time shift for which

$$\left| \lim_{T \rightarrow \infty} \int_{-T}^T B_1(t) [B_2(t + \tau)] dt \right|$$

reaches a maximum. This is a mathematical analogy of the "pulse overlap" method of finding velocity. It may also be referred to as mean or group velocity.

### Ultrasonic Scanning

The alumina samples used for scanning were cut from eight halves of fractured specimens. They were machined into 10- by 20- by 4-mm blocks with parallel sides. One 10- by 20-mm

face on each was polished using a 3- $\mu$ m diamond slurry. This surface condition gave a reflection coefficient which allowed for good attenuation measurements (ref. 8).

A precision acoustic scanning system, described in greater detail elsewhere (ref. 10), was used to scan the samples. Each sample was mounted on a micropositioning table with a transducer fixed above in contact with the sample surface. The transducer had a center frequency of 50 MHz and an approximate beam width of 1 mm. All scans were done over an array of 35 by 15 points; the points were separated by 0.5 mm. The three waveforms,  $FS_2$ ,  $B_1$ , and  $B_2$ , were acquired at each point for later calculation of spectra and images.

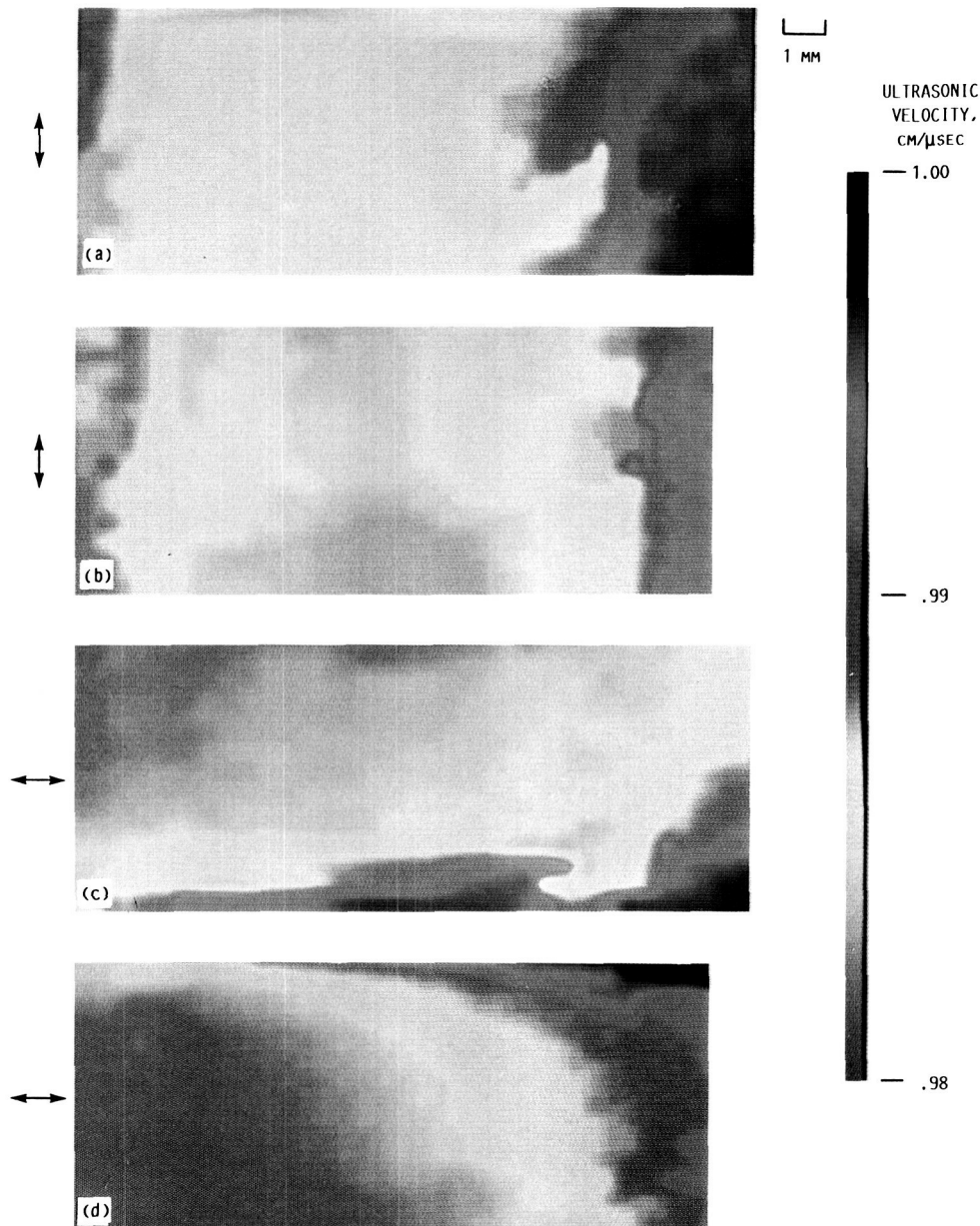
## Results and Discussion

### Velocity Characteristics

The effects of texture can be clearly observed in the composite image of velocity of all eight samples (fig. 5). The averages of velocity and attenuation are found in table III. Averages were determined by using all 525 array points from both samples of each type. Although bulk density is similar for all samples (ref. 1), their structural directionality (texture) is revealed. The samples with notably higher velocity ( $LC$ ) are those for which the direction of sound propagation was the same as the direction of extrusion (longitudinal). Extrusion aligned the grains and crystal axes so that the velocity in the longitudinal direction increased. The elastic modulus was greater than in the isopressed samples (ref. 1), as might be expected. The pore alignment can be observed in the photographs of the fracture surfaces (fig. 3). The pores were also ellipsoidal (table I). The ultrasonic wave traveling in the direction of the extrusion axis "sees" more continuous material, so on the average the energy traveled with higher velocity. There was some variation within each of the  $LC$  images (around 3 percent) where the central region was slightly more porous.

The velocity of both of the isopressed samples ranged only from 0.981 to 0.989  $cm/\mu$ sec, resulting in featureless images. This is not surprising since isopressed samples are expected to be structurally homogeneous and isotropic. The images of the extruded samples were more heterogeneous. The  $RC$  and  $RL$  samples (sound propagation perpendicular to extrusion direction) show variations due to extrusion-caused irregularities. Note that figure 6 includes the same data as figure 5 with a different scale. The maximum value on the scale reference is smaller on figure 6, so the contrast was enhanced. The velocity over these samples ranged from 0.985 to 1.005  $cm/\mu$ sec. The lower velocities indicate lower densities, or more porosity. These samples have bands of varying velocity oriented in the same direction as the extrusion. These bands illustrate grouping of pores during the processes of extrusion and sintering, where differential shrinkage can take place. Grain and pore alignment with the extrusion axis are strikingly apparent in figure 6.





(a) Radial-circumferential *RC* sample 1.  
 (b) Radial-circumferential *RC* sample 2.  
 (c) Radial-longitudinal *RL* sample 1.  
 (d) Radial-longitudinal *RL* sample 2.

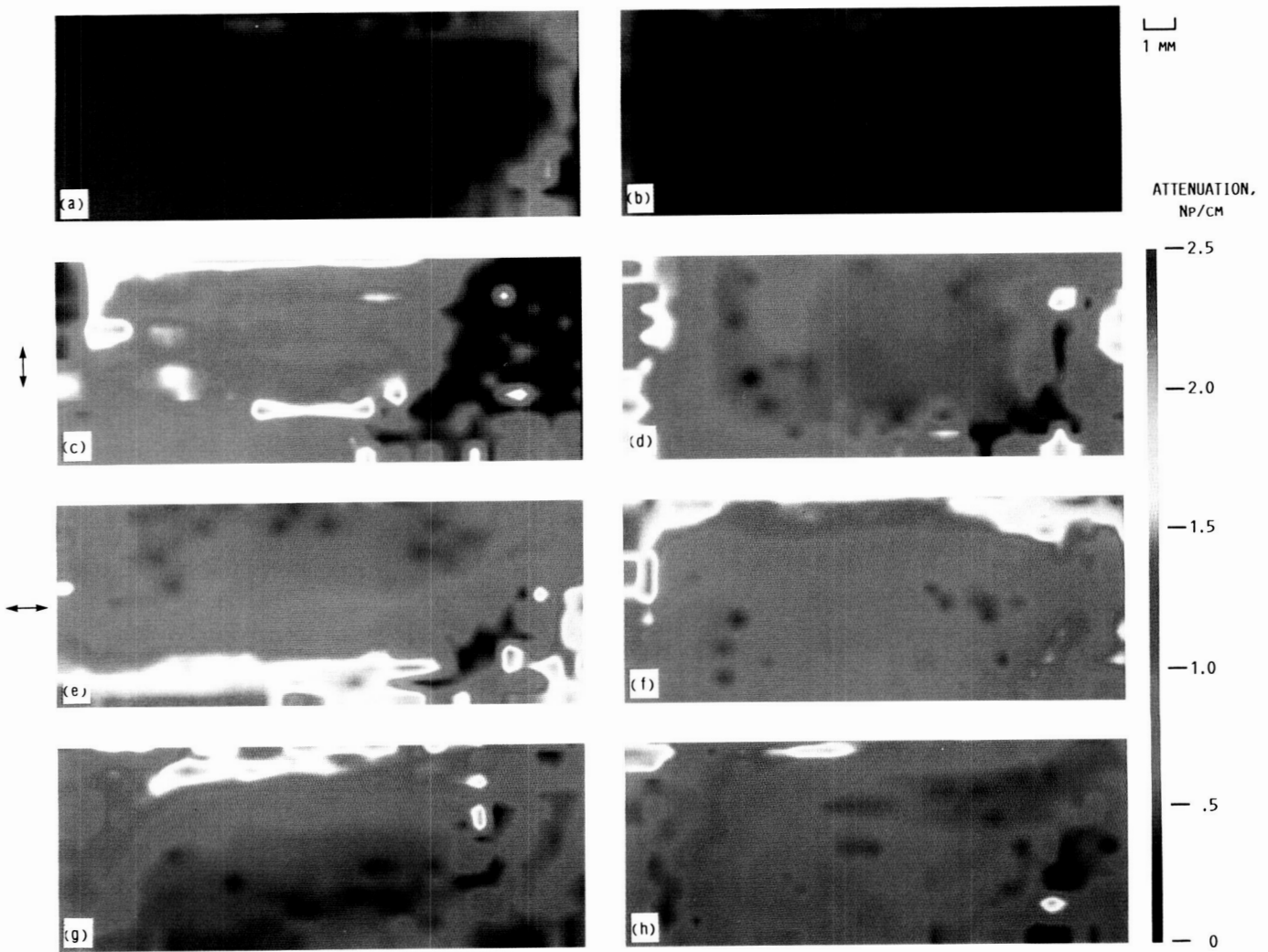
Figure 6.—Velocity images of extruded alumina samples. Arrows indicate axis of extrusion.

### Attenuation Characteristics

Attenuation images of the samples for 50 MHz are shown in figure 7. The isopressed materials exhibited extremely low and uniform attenuation, as seen in figure 7(a) and (b). The extruded samples, however, exhibit a larger range of high attenuation. Within this wide range of attenuation, small regions of uniform attenuation are aligned parallel to the extrusion direction in the *RC* and *RL* orientations (fig. 7(c)

to (f)). These variations indicate regions of varying pore size developed during the extrusion and sintering processes.

Extrusion caused agglomerations of powder particles which densified during sintering. This densification occurred at the expense of the surrounding less dense regions. The ultrasonic energy was scattered by these large pores. Among the three types of extruded samples, the degree of attenuation did not significantly differ. The extrusion caused an increase in velocity along the longitudinal axis but did not cause an



(a) Isopressed sample 1. (b) Isopressed sample 2.  
 (c) Radial-circumferential *RC* sample 1. (d) Radial-circumferential *RC* sample 2.  
 (e) Radial-longitudinal *RL* sample 1. (f) Radial-longitudinal *RL* sample 2.  
 (g) Longitudinal-circumferential *LC* sample 1. (h) Longitudinal-circumferential *LC* sample 1.

Figure 7.—Attenuation images of alumina samples.

attenuation effect dependent on the axis of propagation. These images are consistent with the observation by Generazio (refs. 10 and 12) that often there is high attenuation in areas of velocity gradients. (While the *LC* samples had greater velocity values, velocity variance was similar for all of the extruded samples.)

## Concluding Remarks

Ultrasonic images representing bulk attenuation and velocity of alumina samples were obtained using a pulse-echo contact scanning technique. The samples were taken from larger bodies which varied in that some were isopressed and others were extruded. The larger bodies were mechanically tested,

and crack growth resistance was found to vary with test specimen orientation.

Regions of texture and porosity contribute to the fracture properties in high-temperature ceramic and composite materials (ref. 13). The identification of these regions is therefore of great importance.

The results presented here demonstrate that differences in texture which contribute to variations in structural performance can be revealed by analytic ultrasonic techniques. The scanning technique found ultrasonic velocity and attenuation variations that were related to subtle microstructural differences that controlled fracture properties. Velocity was significantly higher in the samples in which the wave traveled along the axis of extrusion. Areas of high attenuation were found in all of the extruded samples, but no anisotropy similar to the velocity results was observed.

## References

1. Salem, J.A.; Shannon, J.L., Jr.; and Bradt, R.C.: The Effect of Texture on the Crack Growth Resistance of Alumina. NASA TM-100250, 1987.
2. Manderscheid, J.M.; and Gyckenyesi, J.P.: Fracture-Mechanics Concepts in Reliability Analysis of Monolithic Ceramics. Nondestructive Testing of High-Performance Ceramics, A. Vary and J. Snyder, eds., American Ceramic Society, 1987, pp. 59-72. (NASA TM-100174.)
3. Singh, J.P.: A Review of the Effect of Flaws on the Fracture Behavior of Structural Ceramics. ANL/FE-86-3, Sept. 1986.
4. Baaklini, G.Y.; Generazio, E.R.; and Kiser, J.D.: High Frequency Ultrasonic Characterization of Sintered SiC. NASA TM-100825, 1987.
5. Klima, S.J.; and Baaklini, G.Y.: Ultrasonic Characterization of Structural Ceramics. Analytical Ultrasonics in Materials Research and Testing, A. Vary, ed., NASA CP-2383, 1986, pp. 117-126.
6. Davidge, R.W.: The Texture of Special Ceramics with Particular Reference to Mechanical Properties. Proc. Br. Ceram. Soc., no. 20, June 1972, pp. 364-378.
7. Shannon, J.L., Jr.; and Munz, D.: Specimen Size and Geometry Effects on the Fracture Toughness of Aluminum Oxide Measured with Short-Rod and Short-Bar Chevron-Notched Specimens. Chevron-Notched Specimens, Testing and Stress Analysis, ASTM STP-855, J.H. Underwood, S.W. Frieman, and F.I. Baratta, eds., ASTM, Philadelphia, 1984, pp. 270-280.
8. Generazio, E.R.: The Role of the Reflection Coefficient in Precision Measurement of Ultrasonic Attenuation. Mater. Eval., vol. 43, no. 8, July 1985, pp. 995-1004.
9. Hull, D.R.; Kautz, H.E.; and Vary, A.: Measurement of Ultrasonic Velocity Using Phase-Slope and Cross-Correlation Methods. Mater. Eval., vol. 43, no. 11, Oct. 1985, pp. 1455-1460.
10. Generazio, E.R.; Roth, D.J.; and Baaklini, G.Y.: Imaging Subtle Microstructural Variations in Ceramics With Precision Ultrasonic Velocity and Attenuation Measurements. NASA TM-100129, 1987.
11. Bracewell, R.N.: The Fourier Transform and Its Applications. McGraw-Hill, 1974, p. 46.
12. Generazio, E.R.; Stang, D.B.; Roth, D.J.: Dynamic Porosity Variations in Ceramics. Mater. Eval. vol. 46, no. 10, 1988, pp. 1338-1343.
13. Becher, P.F.; and Wei, G.C.: Toughening Behavior in SiC-Whisker-Reinforced Alumina. J. Am. Ceram. Soc., vol. 67, no. 12, Dec. 1984, pp. C267-C269.

TABLE I.—AVERAGE PORE DIMENSIONS RELATIVE TO LONG AXIS

| Specimen processing | Parallel to long axis                 | Perpendicular to long axis |
|---------------------|---------------------------------------|----------------------------|
|                     | Average pore dimension, $\mu\text{m}$ |                            |
| Isopressed          | 8.8                                   | 8.8                        |
| Extruded            | 9.0                                   | 8.0                        |

TABLE II.—TOUGHNESS AND CRACK GROWTH RESISTANCE

| Specimen processing | Toughness, $K_{IC}$ , MPa-m <sup>1/2</sup> | Crack growth resistance, <sup>a</sup> $K_{IR}$ , MPa-m <sup>1/2</sup> |
|---------------------|--|---|
| Isopressed          | 3.67 ± 0.05                                | 2.70  |
| Extruded            |  |   |
| RC                  | 4.94 ± 0.37                                | 4.13  |
| RL                  | 3.99 ± 0.12                                | 3.15  |
| LC                  | 3.63 ± 0.21                                | 2.47  |

<sup>a</sup>Intercept of  $K_{IR}$  versus crack extension curve.

TABLE III.—AVERAGE ULTRASONIC VELOCITY AND ATTENUATION WITH STANDARD DEVIATION

| Specimen processing | Mean velocity, cm/ $\mu\text{sec}$ | Attenuation at 50 MHz, Np/cm |
|---------------------|------------------------------------|------------------------------|
| Isopressed          | 0.985 ± 0.002                      | 0.06 ± 0.17 <sup>a</sup>     |
| Extruded            |                                    |                              |
| RC                  | 0.998 ± 0.003                      | 0.77 ± 0.40                  |
| RL                  | .996 ± 0.004                       | .98 ± 0.56                   |
| LC                  | 1.023 ± 0.003                      | .76 ± 0.42                   |

<sup>a</sup>Probable values ranged from 0.0 to 0.23.



# Report Documentation Page

|   |  |  |  |                            |                   |
|---|--|--|--|----------------------------|-------------------|
| 1. Report No.<br>NASA TM-101478   |  | 2. Government Accession No.                          |  | 3. Recipient's Catalog No. |                   |
| 4. Title and Subtitle<br>Ultrasonic Imaging of Textured Alumina   |  |  | 5. Report Date<br>May 1989   |                            |                   |
|   |  |  | 6. Performing Organization Code  |                            |                   |
| 7. Author(s)<br>David B. Stang, Jonathan A. Salem, and Edward R. Generazio  |  |  | 8. Performing Organization Report No.<br>E-4600  |                            |                   |
|   |  |  | 10. Work Unit No.<br>535-07-01   |                            |                   |
| 9. Performing Organization Name and Address<br>National Aeronautics and Space Administration<br>Lewis Research Center<br>Cleveland, Ohio 44135-3191   |  |  | 11. Contract or Grant No.  |                            |                   |
|   |  |  | 13. Type of Report and Period Covered<br>Technical Memorandum  |                            |                   |
| 12. Sponsoring Agency Name and Address<br>National Aeronautics and Space Administration<br>Washington, D.C. 20546-0001  |  |  | 14. Sponsoring Agency Code   |                            |                   |
|   |  |  | 15. Supplementary Notes<br>David B. Stang, Sverdrup Technology, Inc., NASA Lewis Research Center Group, Cleveland, Ohio 44135;<br>Jonathan A. Salem and Edward R. Generazio, NASA Lewis Research Center. |                            |                   |
| 16. Abstract<br><p>Ultrasonic images representing the bulk attenuation and velocity of a set of alumina samples were obtained by a pulse-echo contact scanning technique. The samples were taken from larger bodies that were chemically similar but were processed by extrusion or isostatic processing. The crack growth resistance and fracture toughness of the larger bodies were found to vary with processing method and test orientation. The results presented here demonstrate that differences in texture that contribute to variations in structural performance can be revealed by analytic ultrasonic techniques.</p> |  |  |  |                            |                   |
| 17. Key Words (Suggested by Author(s))<br>Ultrasonics; Imaging; Alumina; Texture;<br>Nondestructive evaluation; Ultrasonic velocity   |  |  | 18. Distribution Statement<br>Unclassified - Unlimited<br>Subject Category 38  |                            |                   |
| 19. Security Classif. (of this report)<br>Unclassified  |  | 20. Security Classif. (of this page)<br>Unclassified |  | 21. No of pages<br>12      | 22. Price*<br>A03 |